

Online Conformal Probabilistic Numerics via Adaptive Edge-Cloud Offloading

Qiushuo Hou*
qshou@zju.edu.cn

Sangwoo Park^{†‡}
s.park@imperial.ac.uk

Matteo Zecchin[‡]
matteo.1.zecchin@kcl.ac.uk

Yunlong Cai*
ylcai@zju.edu.cn

Guanding Yu*
yuguanding@zju.edu.cn

Osvaldo Simeone[‡]
osvaldo.simeone@kcl.ac.uk

Abstract

Consider an edge computing setting in which a user submits queries for the solution of a linear system to an edge processor, which is subject to time-varying computing availability. The edge processor applies a probabilistic linear solver (PLS) so as to be able to respond to the user’s query within the allotted time and computing budget. Feedback to the user is in the form of a set of plausible solutions. Due to model misspecification, the highest-probability-density (HPD) set obtained via a direct application of PLS does not come with coverage guarantees with respect to the true solution of the linear system. This work introduces a new method to calibrate the HPD sets produced by PLS with the aim of guaranteeing long-term coverage requirements. The proposed method, referred to as online conformal prediction-PLS (OCP-PLS), assumes sporadic feedback from cloud to edge. This enables the online calibration of uncertainty thresholds via online conformal prediction (OCP), an online optimization method previously studied in the context of prediction models. The validity of OCP-PLS is verified via experiments that bring insights into trade-offs between coverage, prediction set size, and cloud usage.

*Zhejiang University

[†]Imperial College London

[‡]King’s College London

1 Introduction

In modern hierarchical computing architectures encompassing edge and cloud servers, the efficient management of computational resources is critical to balance performance with latency and communication overhead. Edge servers process data near the user, providing low-latency, but possibly inaccurate, responses due to limited computational resources. In contrast, cloud servers offer more powerful processing capabilities, but at the cost of introducing communication delays. As an example, in industrial Internet-of-Things (IoT) settings, sensor data processing may leverage both real-time decision-making at the edge and more complex data analytics in the cloud, while accounting for the resulting inherent trade-offs between response speed and accuracy (Hong et al., 2019).

Linear systems serve as the cornerstone of virtually all numerical computation. These systems – in the form of the equation $Ax = b$ with unknown vector x – arise in contexts including convex optimization (Boyd and Vandenberghe, 2004), Kalman filtering for state estimation (Thrun, 2002), and finite element analysis for computational fluid dynamics (Gassner and Winters, 2021). A timely and efficient solution to such systems is often critical for real-time decision-making.

As illustrated in Fig. 1, we consider an edge computing scenario in which, at each round $t = 1, 2, \dots$, a user submits a query for the solution of a linear system $A_t x_t = b_t$ to an edge processor, which is subject to time-varying computing power availability. The user seeks to obtain timely information about the solution $x_t^* = A_t^{-1} b_t$. However, a direct evaluation of the solution requires cubic computational complexity with respect to the matrix dimension, which may be infeasible within the given latency and computing budgets (Wenger and Hennig, 2020; Cockayne et al., 2019a).

Iterative solvers provide an ideal solution to adapt to the available computing budget, as they refine the solution sequentially until the computing budget runs out. *Probabilistic numerics* (PN) (Larkin, 1972) treats numerical problems, such as solving linear systems, as a form of statistical inference. This provides a natural way to quantify the uncertainty associated with iterative numerical solutions obtained under limited computing power.

Specifically, the *probabilistic linear solver* (PLS) (Cockayne et al., 2019a; Hennig et al., 2015; Bartels et al., 2019; Reid et al., 2023; Pfortner et al., 2024) typically treat the solution of a linear system as a Bayesian inference problem, whereby each iteration provides an updated posterior distribution for the solution x_t^* . The posterior distribution reflects the current knowledge of the true solution given the available computing budget. Using this posterior distribution, PLS can construct a *highest-probability-density* (HPD) set \mathcal{C}_t with the aim of covering the true solution x_t^* with a pre-determined target probability level.

In the considered system illustrated in Fig. 1, at each round t , the edge

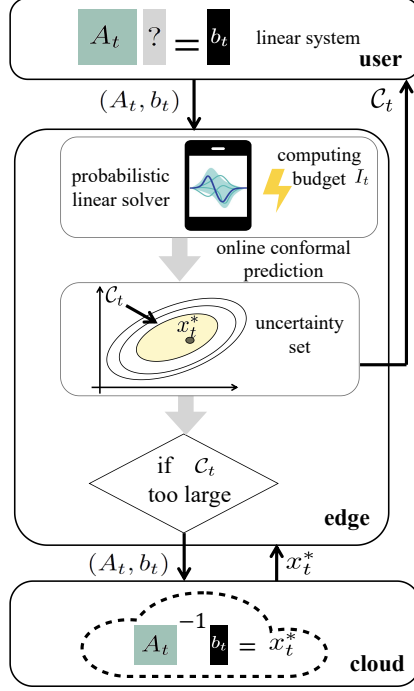


Figure 1: At each round t , a user submits a linear system defined by the pair (A_t, b_t) to an edge device. Given the available computing budget I_t , the edge device employs a probabilistic linear solver (PLS), obtaining a highest-probability-density (HPD) set \mathcal{C}_t for the true solution $x_t^* = A_t^{-1}b_t$. The set \mathcal{C}_t is returned in a timely fashion to the user. The proposed method, OCP-PLS ensures long-term coverage guarantees (2) for the HPD sets \mathcal{C}_t , addressing model misspecification in PLS. To this end, OCP-PLS allows for sporadic communication between cloud and edge.

processor applies PLS so as to be able to respond to the user’s query within the allotted time and computing budgets. Feedback to the user is in the form of a HPD set \mathcal{C}_t . However, in the presence of *model misspecification*, the HPD sets obtained using a direct application of PLS do not come with coverage guarantees with respect to the true solution x_t^* of the linear system (Cockayne et al., 2019a; Bartels et al., 2019; Wenger and Hennig, 2020; Hennig et al., 2015).

Model misspecification arises from the choice of a distribution that does not reflect the properties of the true solution x_t^* . For example, one typically assumes a Gaussian prior, but the solution x_t^* may be sparse. Misspecification may also arise due to simplifications done in the evaluation of the likelihood in order to obtain Gaussian posteriors, as is the case with BayesCG (Hegde et al., 2025; Reid et al., 2023; Wenger and Hennig, 2020; Cockayne et al., 2019a, 2022, 2019b), which may reinforce incorrect prior assumptions.

Further work on the impact of calibration on PLS includes reference (Reid et al., 2023), which demonstrated that BayesCG search directions yield a slightly optimistic HPD set under the Krylov prior, and references (Hegde et al., 2025; Cockayne et al., 2021), which explored the use of probabilistic stationary iterative methods rather than Bayesian framework.

This work introduces a new method to calibrate the HPD sets produced by PLS with the aim of guaranteeing long-term coverage requirements. In practice, we wish to ensure that, on average over time, the HPD set \mathcal{C}_t returned by the edge to the user contains the true solution x_t^* with a user-defined *coverage* rate $1 - \alpha$.

To ensure this condition, we assume that, *sporadically*, the edge processor can submit the current linear system defined by the pair (A_t, b_t) to a cloud processor. This offloading to the cloud is done after responding to a user’s query in order not to affect the latency experienced by the user. When submitting the job to the cloud, the edge processor receives the true solution x_t^* . This information can be used to monitor the current coverage rate, making it possible to calibrate the prediction sets \mathcal{C}_t towards meeting the required target rate $1 - \alpha$.

The proposed method, referred to as *online conformal prediction-PLS* (OCP-PLS), integrates for the first time PLS with *online conformal prediction* (OCP), an online optimization method previously studied in the context of predictive models (Gibbs and Candes, 2021; Angelopoulos et al., 2024). The theoretical validity of OCP-PLS is verified via experiments that bring insights into trade-offs between coverage, prediction set size, and cloud usage.

The structure of the paper is as follows. Section 2 introduces the problem of conformal PLS. The necessary background on OCP is reviewed in Section 3. Section 4 presents the proposed approaches for constructing OCP-PLS. Simulation results are summarized in Section 5. Finally, Section 6 concludes the paper.

2 Setting and Problem Formulation

In this section, we define the problem studied in this paper.

2.1 Setting and Problem Definition

As illustrated in Fig. 1, we study a hierarchical computing architecture encompassing edge and cloud processors. At each round t , a user submits a linear system problem defined by the pair (A_t, b_t) , consisting of an $n_t \times n_t$ Hermitian matrix A_t and an $n_t \times 1$ vector b_t , to the edge device. The user is interested in obtaining information about the solution

$$x_t^* = A_t^{-1}b_t. \quad (1)$$

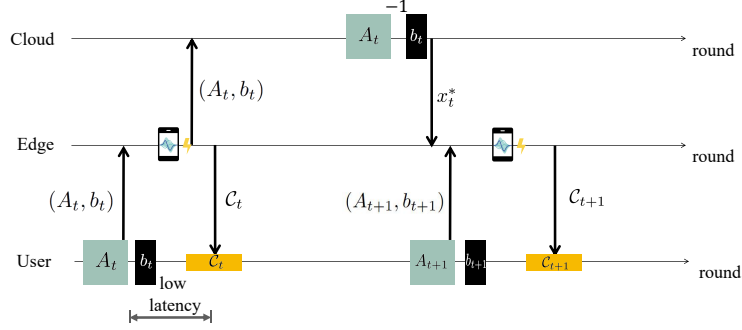


Figure 2: Timeline of messages exchanged across cloud, edge, and user.

This solution is supposed to exist and to be unique, requiring matrix A_t to be invertible. Problems of this type are common in a wide variety of applications, such as convex optimization using Newton’s method requiring Hessian matrix inversion (Boyd and Vandenberghe, 2004), Kalman filtering for state estimation (Thrun, 2002), and partial differential equations in computational fluid dynamics via Galerkin’s method (Gassner and Winters, 2021).

At each round t , the edge has available a computing budget I_t . Accounting for this limited budget, the edge device employs PLS to obtain an HPD set \mathcal{C}_t for the true solution (1) (Cockayne et al., 2019a; Bartels et al., 2019; Wenger and Hennig, 2020). This set is returned to the user in response to its query. Thanks to processing at the edge, the user’s requests experience low latency (see Fig. 2).

This paper addresses the problem of *calibrating* the prediction set \mathcal{C}_t so as to ensure that the sequence of HPD sets \mathcal{C}_t returned to the user satisfies the following long-term coverage condition

$$\left| \frac{1}{T} \sum_{t=1}^T \Pr\{x_t^* \in \mathcal{C}_t\} - (1 - \alpha) \right| = o(1), \quad (2)$$

where $\alpha \in [0, 1]$ is a pre-determined target miscoverage level, and $o(1)$ denotes a quantity that tends to zero as $T \rightarrow \infty$. The probability (2) is evaluated over the randomness associated with edge-cloud communication, as it will be described in Section 4. By (2), a fraction approximately equal to $1 - \alpha$ of the prediction sets contains the true solution x_t^* .

As shown in Fig. 2, after responding to the user, the edge processor analyzes the prediction set \mathcal{C}_t , and decides whether to submit the problem (A_t, b_t) for validation to the cloud. If the edge processor communicates the pair (A_t, b_t) to the cloud, the cloud evaluates the true solution x_t^* and returns it to the edge. This allows the edge to monitor the condition (2), and to calibrate future sets $\mathcal{C}_{t'}$ with $t' > t$. However, cloud-based validation is

expensive, and the edge aims at keeping the number of problems submitted to the cloud as low as possible. As shown in Fig. 2, we will assume first that feedback from the cloud, if requested, is received prior to the next query (A_{t+1}, b_{t+1}) by the user. This assumption will be alleviated in the appendix.

2.2 Probabilistic Linear Solver

As previously mentioned, the edge processor addresses the problem (A_t, b_t) within the computing budget I_t using PLS. Accordingly, PLS treats the solution of a linear system as a Bayesian inference problem. This enables the quantification of the uncertainty associated with numerical solutions obtained within a limited computing budget (Cockayne et al., 2019a; Bartels et al., 2019; Wenger and Hennig, 2020).

Given a budget of I_t iterations, PLS operates sequentially by considering at each iteration $i = 1, \dots, I_t$ a *search direction* s_i , yielding an effective observation $y_i = s_i^T b$. Given a Gaussian prior distribution $x^* \sim \mathcal{N}(\mu_0, \Sigma_0)$ on the solution $x^* = A_t^{-1} b_t$ with a full-rank diagonal matrix Σ_0 , PLS returns the Gaussian posterior

$$p(x_t | y_1, \dots, y_{I_t}; A_t, b_t) = \mathcal{N}(x_t | \mu_t, \Sigma_t) \quad (3)$$

obtained from the observations y_1, \dots, y_{I_t} . In (3), the $d \times 1$ mean vector μ_t and the $d \times d$ covariance matrix Σ_t are evaluated as (Cockayne et al., 2019a; Bartels et al., 2019)

$$\begin{aligned} \mu_t &= \mu_0 + \Sigma_0 A_t S_t (S_t^\top A_t \Sigma_0 A_t S_t)^{-1} S_t^\top (b - A_t \mu_0), \\ \Sigma_t &= \Sigma_0 - \Sigma_0 A_t S_t (S_t^\top A_t \Sigma_0 A_t S_t)^{-1} S_t^\top A_t \Sigma_0, \end{aligned} \quad (4)$$

with the $d \times I_t$ matrix

$$S_t = [s_1, \dots, s_{I_t}] \quad (5)$$

collecting the I_t search directions. Note that the covariance matrix Σ_t has rank

$$r_t \leq n_t - I_t, \quad (6)$$

with equality achieved if the directions S_t are suitably chosen (Wenger et al., 2022). Note also that, due to the propagation of floating point error, the rank r_t may be practically larger than $n_t - I_t$. This may be the case, e.g., when using BayesCG as the search directions and the number of iterations I_t is close to the dimension n_t (Cockayne et al., 2019a).

Given the posterior distribution (3), an $(1 - \alpha)$ -HPD set for the true solution x_t^* can be obtained as

$$\begin{aligned} \mathcal{C}_t &= \operatorname{argmin}_{\mathcal{C} \subseteq \mathbb{R}^d} |\mathcal{C}| \\ \text{s.t. } &\int_{x_t \in \mathcal{C}} p(x_t | A_t, b_t) dx_t \geq 1 - \alpha, \end{aligned} \quad (7)$$

where we wrote $p(x_t|A_t, b_t)$ in lieu of $p(x_t|y_1, \dots, y_{I_t}; A_t, b_t)$ to simplify the notation.

The HPD set (7) covers the true solution x_t^* in (1) with probability no smaller than $1 - \alpha$, i.e.,

$$\Pr[x_t^* \in \mathcal{C}_t] \geq 1 - \alpha, \quad (8)$$

only if the posterior distribution $p(x_t|A_t, b_t)$ accurately quantifies the uncertainty associated with estimating the solution x_t^* given the observation y_1, \dots, y_{I_t} . Accordingly, the posterior distribution $p(x_t|A_t, b_t)$ is regarded as *well calibrated* when the coverage probability in (8) equals the target level $1 - \alpha$.

However, the PLS posterior (3) is known to be generally poorly calibrated because of model misspecification (Cockayne et al., 2019a; Bartels et al., 2019; Wenger and Hennig, 2020; Hennig et al., 2015). Therefore, there is a need to develop model selection to satisfy the coverage requirement (2). This is the main objective of this work.

3 Background

This section reviews the necessary background on OCP (Gibbs and Candes, 2021; Zhao et al., 2024).

3.1 Online Conformal Prediction

Given an arbitrary sequence of input-output pairs $(x_t, y_t) \in \mathcal{X} \times \mathcal{Y}$, for $t = 1, 2, \dots$, OCP aims to construct a prediction set $\mathcal{C}_t(x_t)$ on the output space \mathcal{Y} that satisfies long-term coverage guarantees. OCP builds on a scoring function $s : \mathcal{X} \times \mathcal{Y} \rightarrow \mathbb{R}$ that measures the extent to which the output y is mismatched to the input x . A smaller value $s(x, y)$ indicates that y is a better fit for input x . The set $\mathcal{C}_t(x_t)$ is obtained by choosing all the candidate output values $y \in \mathcal{Y}$ with sufficiently small scores $s(x, y)$, i.e.,

$$\mathcal{C}_t(x_t) = \{y \in \mathcal{Y} : s(x_t, y) \leq \lambda_t\}, \quad (9)$$

where λ_t is a threshold.

OCP updates the threshold λ_t in (9) based on the input-output pairs $(x_1, y_1), \dots, (x_{t-1}, y_{t-1})$ with the aim of ensuring the long-term coverage condition

$$\left| \frac{1}{T} \sum_{t=1}^T \mathbb{1}\{y_t \in \mathcal{C}_t(x_t)\} - (1 - \alpha) \right| \leq \frac{C}{T}, \quad (10)$$

where C is a constant independent of T . This result is obtained by updating the threshold as

$$\lambda_{t+1} = \lambda_t + \gamma(\mathbb{1}\{y_t \notin \mathcal{C}_t(x_t)\} - \alpha), \quad (11)$$

where $\gamma > 0$ is a step size. This update rule intuitively increases the threshold when the prediction set $\mathcal{C}_t(x_t)$ fails to cover the true outcome y_t , making future sets more conservative, while decreasing it when coverage is achieved, making future sets more efficient.

The validity of the condition (10) for the prediction sets (9) obtained via the OCP update rule (11) were shown in Gibbs and Candes (2021) using a telescoping argument, obtaining

$$C = \max \frac{|\lambda_{T+1} - \lambda_1|}{\gamma}. \quad (12)$$

If the score function $s(x, y)$ is bounded within the interval $[m, M]$ with $M > m$ for any $(x, y) \in \mathcal{X} \times \mathcal{Y}$, then the threshold λ_t can be also proved to be bounded as $\lambda_t \in [m - \gamma\alpha, M + \gamma(1 - \alpha)]$, where λ_1 is selected within the interval $[m, M]$ (Gibbs and Candes, 2021; Feldman et al., 2022). Accordingly, the quantity (12) is given as

$$C = \frac{M - m + \gamma}{\gamma}, \quad (13)$$

which does not depend on T .

3.2 Intermittent Online Conformal Prediction

The OCP update (11) requires *dense* feedback, as it assumes the availability of the true output y_t at every time step $t = 1, 2, \dots$ in (11). Intermittent OCP (I-OCP) (Zhao et al., 2024) alleviates this assumption by leveraging inverse probability weighting, also known as the Horvitz–Thompson estimator, which is used in statistical inference with missing data (Imbens and Rubin, 2015).

Specifically, I-OCP assumes that the output y_t is available with probability p_t . The availability of the output is thus described by a Bernoulli random variable $\text{obs}_t \sim \text{Bern}(p_t)$, which indicates the availability of the output value y_t if $\text{obs}_t = 1$, and its absence when $\text{obs}_t = 0$. The variables obs_t are independent over the time index t . The update rule applied by I-OCP is given by

$$\lambda_{t+1} = \lambda_t + \frac{\gamma}{p_t} (\mathbb{1}\{y_t \notin \mathcal{C}_t(x_t)\} - \alpha) \cdot \text{obs}_t. \quad (14)$$

Thus, I-OCP amplifies the update of the threshold to an extent that is inversely proportional to the availability probability p_t . Accordingly, when feedback is less likely, i.e., when p_t is smaller, the effective step size is increased to compensate for possible missing data.

It can be proved that I-OCP satisfies the long-term expected coverage property (Zhao et al., 2024)

$$\left| \frac{1}{T} \sum_{t=1}^T \Pr [y_t \in \mathcal{C}_t(x_t)] - (1 - \alpha) \right| \leq \frac{C}{T} \quad (15)$$

with C in (12), where the probability is evaluated over the randomness of the Bernoulli random variables $\text{obs}_1, \dots, \text{obs}_T$.

In a manner similar to OCP, as long as the score function $s(x, y)$ is bounded in the interval $[m, M]$ for any $(x, y) \in \mathcal{X} \times \mathcal{Y}$, it can be shown that the quantity C in (15) is also bounded. Specifically, denote as p_t^{\min} the lowest value that can be attained by the probability p_t . Note that the probability p_t can generally depend on the previous history $(x_1, y_1), \dots, (x_{t-1}, y_{t-1})$. Then, the threshold λ_t is bounded as

$$\lambda_t \in \left[m - \gamma \frac{\alpha}{\min_{t'=1, \dots, t-1} p_{t'}^{\min}}, M + \gamma \frac{1 - \alpha}{\min_{t'=1, \dots, t-1} p_{t'}^{\min}} \right] \quad (16)$$

as long as one sets $\lambda_1 \in [m, M]$. Accordingly, we have

$$C = \frac{M - m}{\gamma} + \frac{1}{\bar{p}_T}, \quad (17)$$

for any

$$\bar{p}_T = \min_{t=1, \dots, T} p_t^{\min}. \quad (18)$$

This quantity does not depend on T if a strictly positive \bar{p} exists with

$$\bar{p}_T \geq \bar{p} \quad (19)$$

for all times T .

4 Online Conformal Probabilistic Linear Solver

In this section, we present OCP-PLS, a novel framework for edge inference via PN that satisfies the long-term quality-of-service requirement (2) by integrating PLS (see in Section 2.2) with I-OCP (see Section 3).

4.1 Score Function

As discussed in Section 3.1, OCP requires the definition of a score function for any value of the target variable. In the setting described in Section 2, the target variable at each time t is the true solution x_t^* in (1). Given the posterior distribution (3)-(4) produced by PLS, we set the score for any candidate solution x_t to be proportional to the density of the scaled degenerate multivariate Gaussian distribution $\mathcal{N}(x_t | \mu_t, \Sigma_t)$. Let $\Sigma_t = V_t \Lambda_t V_t^T$ be

the eigendecomposition of the rank- r_t covariance matrix Σ_t , where V_t is a unitary $n_t \times r_t$ matrix and Λ_t is an $r_t \times r_t$ diagonal matrix. The score can be explicitly written as

$$s(x_t; A_t, b_t) = \begin{cases} \exp(-(x_t - \mu_t)^T V_t \Lambda_t^{-1} V_t^T (x_t - \mu_t)) & \text{if } (x_t - \mu_t) \in \text{range}(\Sigma_t), \\ 0 & \text{otherwise.} \end{cases} \quad (20)$$

By doing this, the score function is bounded between 0 and 1.

Since matrix Σ_t in (4) can be expressed as a sequence of rank-1 updates to the prior diagonal matrix Σ_0 , its eigendecomposition can be efficiently updated using Given's rotations (Golub and Van Loan, 2013, Section 12.5). This results in a per-iteration complexity of $\mathcal{O}(n_t^2)$, and an overall complexity of $\mathcal{O}(I_t n_t^2)$ after I_t updates. Note that the score (20) depends on the specific sequence of search directions (5), although we do not make this dependence explicit in the notation $s(x_t; A_t, b_t)$.

Equipped with the scoring function (20), OCP-PLS produces a prediction set of the form

$$\mathcal{C}_t = \{x_t \in \mathbb{R}^d : s(x_t; A_t, b_t) \geq \lambda_t\}, \quad (21)$$

with a suitably designed threshold λ_t .

Two observations are in order about the OCP-PLS set (21). First, the PLS set (7) can be seen to take the same form as (21). However, PLS selects the threshold λ_t by imposing the constraint in (7), which satisfies the requirement (2) only if the model is well specified. In contrast, as discussed in Section 4.2, OCP-PLS sets the threshold λ_t by following the principles of OCP (see Section 3).

4.2 Cloud-to-Edge Feedback and Threshold Selection

As illustrated in Fig. 1 and Fig. 2, in order to set the threshold λ_t in (21), OCP-PLS leverages sporadic feedback from the cloud to the edge. Specifically, we propose to submit a query (A_t, b_t) to the cloud with a probability p_t that increases with the *volume radius* of the set \mathcal{C}_t , i.e., with $|\mathcal{C}_t|^{1/r_t}$ where

$$|\mathcal{C}_t| = \frac{\pi^{r_t/2}}{\Gamma(r_t/2 + 1)} \cdot |\Lambda_t|^{1/2} \cdot (-\log \lambda_t)^{r_t/2}, \quad (22)$$

with $\Gamma(\cdot)$ being the Gamma function. In this way, cloud-to-edge feedback is more likely to be requested at time instants t characterized by a larger uncertainty, hence making cloud feedback more valuable for calibration. Conversely, when the HPD set is small enough, we reduce the probability of requesting feedback, thereby saving cloud computing resources.

While any normalized increasing function of the set size $|\mathcal{C}_t|$ can be used to design p_t , we adopt the sigmoid function $\sigma(x) = (1 + \exp(-x))^{-1}$ and set

as

$$p_t = \sigma \left(\frac{\log |\mathcal{C}_t|}{r_t} - \theta \right), \quad (23)$$

which acts as a soft threshold on the log-volume radius. Lower values of the threshold θ in (23) increase the probability of cloud-to-edge feedback, yielding a smaller set \mathcal{C}_t at the cost of higher usage of cloud resources.

Leveraging the feedback from the cloud, OCP-PLS targets the requirement (2) by updating the threshold according to the rule

$$\lambda_{t+1} = \lambda_t - \frac{\gamma}{p_t}(\text{err}_t - \alpha) \cdot \text{obs}_t, \quad (24)$$

where the error at round t is defined as

$$\text{err}_t = \mathbb{1}\{x_t^* \notin \mathcal{C}_t\}. \quad (25)$$

The rule (24) is aligned with the I-OCP update (14). As formalized next, this ensures the validity of the coverage condition (2). The overall OCP-PLS procedure is summarized in Algorithm 1.

Algorithm 1 OCP-PLS

```

1: set hyperparameters  $\lambda_1 \in [0, 1]$ ,  $\gamma$ ,  $\theta$  ▷ initialization
2: for  $t = 1, 2, \dots, T$  do
3:   apply PLS with  $I_t$  iterations to evaluate  $\mu_t$  and  $\Sigma_t$  in (4)
4:   evaluate the probability  $p_t$  in (23)
5:   draw  $\text{obs}_t \sim \text{Bern}(p_t)$ 
6:   evaluate the HPD set  $\mathcal{C}_t$  in (21)
7:   if  $\text{obs}_t = 1$  then
8:     obtain  $x_t^*$  from the cloud
9:      $\text{err}_t = \mathbb{1}\{s(x_t^*; A_t, b_t) < \lambda_t\}$ 
10:     $\lambda_{t+1} = \lambda_t - \frac{\gamma}{p_t}(\text{err}_t - \alpha)\text{obs}_t$  ▷ update  $\lambda_t$ 
11:   else
12:      $\lambda_{t+1} = \lambda_t$ 
13:   end if
14: end for
```

4.3 Theoretical Coverage Guarantee

OCP-PLS ensures condition (2) in the following way.

Proposition 1. *Assume that there exists a strictly positive probability \bar{p} satisfying the inequality (19) for all times T . Then, OCP-PLS satisfies the long-term coverage property*

$$\left| \frac{1}{T} \sum_{t=1}^T \Pr [x_t^* \in \mathcal{C}_t] - (1 - \alpha) \right| \leq \frac{C}{T}, \quad (26)$$

with constant

$$C = \frac{1}{\gamma} + \frac{1}{\bar{p}}. \quad (27)$$

Proof. This result follows directly from Section 3.2 by noting that $s(x_t; A_t, b_t)$ in (20) is bounded in $[0, 1]$. \square

5 Experiments

This section evaluates the performance of the proposed OCP-PLS scheme via numerical experiments.

5.1 Setup

At each round t , we randomly and independently generate a Hermitian matrix A_t as $A_t = Q_t \Lambda_t Q_t$, where $n_t \times n_t$ orthogonal matrix Q_t follows the Haar distribution and the diagonal matrix Λ_t has diagonal elements drawn from a Gamma distribution with shape parameter 10, scale parameter 1, and location parameter 0. The dimension n_t is drawn i.i.d. and uniformly from the interval $[500, 1000]$. Furthermore, each element of vector b_t is sampled i.i.d. from the standard multivariate Gaussian distribution. We use the prior $x \sim \mathcal{N}(0, I)$, and BayesCG for the search directions (Cockayne et al., 2019b).

We set the target miscoverage rate α as 0.1. The step size γ and initial threshold λ_1 are set as 0.05 and 0.99, respectively. For the hyperparameter θ , we use grid search to find a suitable one as -3.5 .

We consider two different scenarios in terms of edge processing power availability:

- **Constant edge computing budget:** In this case, the computing budget is set as a fixed fraction of the problem size as $I_t = 0.1n_t$.
- **Time-varying edge computing budget:** In this more challenging scenario, the number of allowed iterations starts at $I_t = 0.1n_t$ for $t = 1$ to $t = 1500$, then it decreases to $I_t = 0.005n_t$ for $t = 1500$ to $t = 3500$, and finally it increases to $I_t = 0.15n_t$ for $t = 3500$ to $t = 5000$.

5.2 Baselines

We consider the following baselines:

- **PLS:** Conventional PLS directly adopts the $(1 - \alpha)$ -HPD set as in (7).
- **OCP-PLS with full cloud-to-edge feedback:** This corresponds to the proposed OCP-PLS method with probability $p_t = 1$ of acquiring feedback from cloud to edge.

5.3 Performance Metrics

As performance measures, we report empirical coverage, empirical HPD set size, and empirical cloud-to-edge feedback rate evaluated on a sequence $\{A_t, b_t\}_{t=1}^T$ of duration $T = 5000$. The empirical coverage at round t measures the fraction of times in which the exact solution x_τ^* was included in the corresponding HPD set \mathcal{C}_t from time $\tau = 1$ until time $\tau = t$, i.e.,

$$\text{empirical coverage} = \frac{1}{t} \sum_{\tau=1}^t \mathbb{1}\{x_\tau^* \in \mathcal{C}_\tau\}. \quad (28)$$

The size of the HDP set is measured by the empirical volume radius as

$$\text{empirical volume radius} = \frac{1}{t} \sum_{\tau=1}^t |\mathcal{C}_\tau|^{1/r_\tau}. \quad (29)$$

Finally, the empirical cumulative cloud-to-edge feedback rate is defined as

$$\text{empirical cumulative cloud-to-edge feedback rate} = \sum_{\tau=1}^t \text{obs}_\tau. \quad (30)$$

We average the probability (28)-(30) over 10 independent experiments.

5.4 Results

In this subsection, we evaluate coverage, average set size, and cumulative cloud-to-edge feedback rate starting from the case with a constant edge computing budget.

Fig. 3(a) demonstrates that both OCP-PLS and OCP-PLS with full cloud-to-edge feedback guarantee the long-term coverage condition (2), thereby validating Proposition 1. In contrast, confirming prior art (Hegde et al., 2025; Wenger and Hennig, 2020), PLS produces an overly conservative HPD set that always covers the true solution. PLS achieves coverage of 1 by yielding much larger HPD sets than both OCP-PLS and OCP-PLS with full cloud-to-edge feedback, as shown in Fig. 3(b). Furthermore, as illustrated in (2), OCP-PLS can reduce the cloud-to-edge feedback rate by approximately 40% as compared to OCP-PLS with full cloud-to-edge feedback, while producing sets with similar sizes.

Consider now the setting with a time-varying computing budget at the edge. Fig. 4 marks the times at which the computing budget changes with vertical dashed lines. Fig. 4(a) verifies that both OCP-PLS and OCP-PLS with full cloud-to-edge feedback maintain the guaranteed long-term coverage condition proved in Proposition 1 even under time-varying computing budgets. As in the previous example, PLS provides perfect coverage at

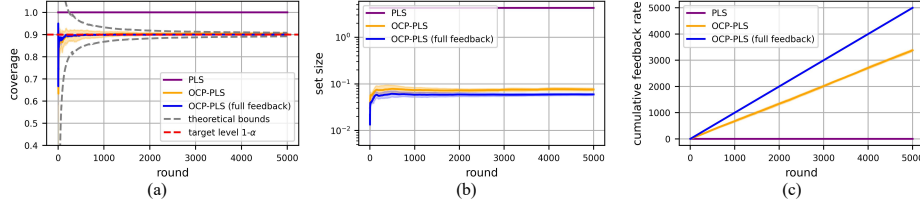


Figure 3: Coverage (a), set size (b), and cumulative cloud-to-edge feedback rate (c) for PLS, OCP-PLS, and OCP-PLS with full cloud-to-edge feedback for target coverage level $1 - \alpha = 0.9$ (red dashed line in (a)). The gray dashed line in (a) corresponds to the threshold bound (15).

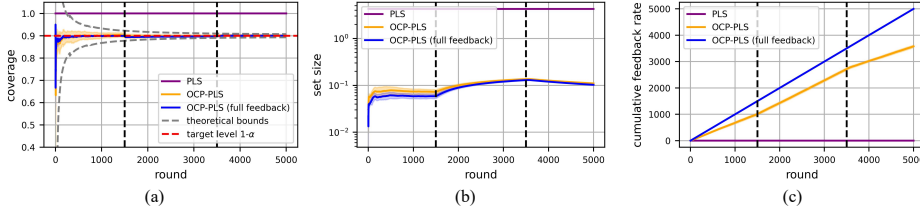


Figure 4: Coverage (a), set size (b), and cumulative cloud-to-edge feedback rate (c) for PLS, OCP-PLS, and OCP-PLS with full cloud-to-edge feedback for target coverage level $1 - \alpha = 0.9$ (red dashed line in (a)) in a setting with time-varying edge computing budget. The gray dashed line in (a) corresponds to the threshold bound (15).

the cost of excessively large HPD sets. In contrast, as shown in Fig. 4(b), OCP-PLS responds naturally to changes in edge computing budget, as the set sizes increase during periods of reduced computing budget ($t = 1500$ to $t = 3500$), while decreasing when the computing budget is higher ($t = 3500$ to $t = 5000$). Throughout these variations, OCP-PLS consistently maintains a significantly lower cloud-to-edge feedback rate than OCP-PLS with full cloud-to-edge feedback, as shown in Fig. 4(c), adapting the feedback rate to the varying computing budgets. This demonstrates OCP-PLS’s ability to balance reliability and communication efficiency under dynamic edge computing budgets.

6 Conclusion

An important challenge in edge-cloud computing architectures is to provide users with timely and reliable responses under limited computational budgets. This work has made steps towards addressing this challenge by leveraging probabilistic numerics (PN) and online conformal prediction (OCP), an online calibration method previously studied in the context of predictive

models. The proposed methodology, referred to as OCP-PLS calibrates the HPD sets produced by probabilistic linear solvers (PLS), ensuring provable coverage guarantees for the true solution. OCP-PLS supports an adaptive mechanism for the use of cloud resources that reduces the communication overhead between edge and cloud, as well as the computational load of the cloud processors. Experiments for tasks requiring the sequential solution of linear systems validate the theoretical reliability, as well as the efficiency, of OCP-PLS. Future work may investigate the generalization of the proposed approach to other numerical problems beyond linear systems (Wenger et al., 2022; Pfortner et al., 2022; Hegde et al., 2025).

Appendix A: Extension to Delayed Cloud-to-Edge Feedback

In this appendix, we extend the analysis of OCP-PLS to a setting with delayed cloud-to-edge feedback. Specifically, we assume that, given a request to the cloud at the t -th time instant, the corresponding cloud-to-edge feedback may not arrive before the $(t+1)$ -th request from the user. We denote as d_t the corresponding feedback delay, i.e., the feedback arrives right before serving the $(t+1+d_t)$ -th time instant and after the $(t+d_t)$ -th time instant, where $d_t \geq 1$ is an integer. Note that the case $d_t = 0$ corresponds to the setting considered in Section 2.

A direct extension of the threshold update rule (24) is obtained by updating the threshold whenever the edge receives feedback from the cloud. This can be written as

$$\lambda_{t+1} = \lambda_t - \gamma \sum_{t' \in \mathcal{T}_t} \frac{\text{obs}_{t'}}{p_{t'}} (\mathbb{1}\{x_{t'}^* \notin \mathcal{C}_{t'}\} - \alpha), \quad (31)$$

where the set \mathcal{T}_t is defined as

$$\mathcal{T}_t = \{t' : t' + d_{t'} = t\}. \quad (32)$$

We will now impose mild assumptions on the delays d_t so as to ensure the validity of OCP-PLS. Specifically, we assume the inequality

$$t + d_t \leq t' + d_{t'} \quad (33)$$

for all $t < t'$, so that the feedback signals are received in the same order as the requests are sent to the cloud. We also assume that the cardinality of the set \mathcal{T}_t is bounded as

$$|\mathcal{T}_t| \leq T^{\max} \quad (34)$$

for some finite integer T^{\max} .

Proposition 2. Assume that there exists a strictly positive probability \bar{p} satisfying the inequality (19) for all times $T + T^{\max}$. Then, for any fixed sequence of delays d_1, d_2, \dots , that ensure assumptions (33)-(34), the OCP-PLS update rule (31) guarantees the long-term expected coverage property

$$\left| \frac{1}{T} \sum_{t=1}^T \Pr[x_t^* \in \mathcal{C}_t] - (1 - \alpha) \right| \leq \frac{C}{T}, \quad (35)$$

with constant

$$C = T^{\max} - 1 + \frac{1}{\gamma} + \frac{T^{\max}}{\bar{p}}. \quad (36)$$

Note that Proposition 2 reduces to Proposition 1 in Section 4.3 by setting $T^{\max} = 1$ and $d_t = 0$, i.e., when there is no delay in the cloud-edge feedback.

Proof. Taking the expectation on the both sides of equation (31) and using a telescoping argument for $t = 1, \dots, T + d_T + 1$, we get

$$\begin{aligned} \mathbb{E}[\lambda_{T+d_T+1}] &= \lambda_1 - \gamma \sum_{t'=1}^{T+d_T} \sum_{t \in \mathcal{T}_{t'}} (\Pr[x_t^* \notin \mathcal{C}_t] - \alpha), \\ &= \lambda_1 - \gamma \sum_{t=1}^{T'} (\Pr[x_t^* \notin \mathcal{C}_t] - \alpha), \end{aligned} \quad (37)$$

where $T' = \max\{t \in \mathcal{T}_{T+d_T}\}$ is the index of the most recent cloud-to-edge feedback used to update λ_{T+d_T+1} .

The expected coverage up to time T' can be obtained as

$$\frac{1}{T'} \sum_{t=1}^{T'} \Pr[x_t^* \in \mathcal{C}_t] = 1 - \alpha - \frac{\mathbb{E}[\lambda_{T+d_T+1}] - \lambda_1}{T' \gamma}. \quad (38)$$

Based on (38), we express the expected coverage up to time T is follows

$$\begin{aligned} \frac{1}{T} \sum_{t=1}^T \Pr[x_t^* \in \mathcal{C}_t] &= \frac{T'}{T} \frac{1}{T'} \sum_{t=1}^{T'} \Pr[x_t^* \in \mathcal{C}_t] - \frac{1}{T} \sum_{t=T+1}^{T'} \Pr[x_t^* \in \mathcal{C}_t], \\ &\stackrel{(a)}{=} \frac{T'}{T} (1 - \alpha) - \frac{\mathbb{E}[\lambda_{T+d_T+1}] - \lambda_1}{T \gamma} - \frac{1}{T} \sum_{t=T+1}^{T'} \Pr[x_t^* \in \mathcal{C}_t], \\ &= (1 - \alpha) + \frac{(T' - T) \cdot (1 - \alpha) - \sum_{t=T+1}^{T'} \Pr[x_t^* \in \mathcal{C}_t]}{T} \\ &\quad - \frac{\mathbb{E}[\lambda_{T+d_T+1}] - \lambda_1}{T \gamma}, \end{aligned} \quad (39)$$

where (a) uses (38). The coverage gap can be bounded as

$$\begin{aligned} &\left| \frac{1}{T} \sum_{t=1}^T \Pr[x_t^* \in \mathcal{C}_t] - (1 - \alpha) \right| \\ &\leq \frac{|(T' - T) \cdot (1 - \alpha) - \sum_{t=T+1}^{T'} \Pr[x_t^* \in \mathcal{C}_t]|}{T} + \frac{|\mathbb{E}[\lambda_{T+d_T+1}] - \lambda_1|}{T \gamma}, \end{aligned} \quad (40)$$

with the first term on the right-hand side appearing due to the presence of a delay in the cloud-edge feedback. From Assumption (35), it follows that $T' - T \leq T^{\max} - 1$, and therefore we can bound this term as

$$\left| (T' - T) \cdot (1 - \alpha) - \sum_{t=T+1}^{T'} \Pr[x_t^* \in \mathcal{C}_t] \right| \leq T^{\max} - 1. \quad (41)$$

Using a proof technique similar to the one used without delayed feedback in Section 3, given a score function $s(x, y)$ that is bounded in the interval $[0, 1]$ for any $(x, y) \in \mathcal{X} \times \mathcal{Y}$, the threshold λ_t obtained via (31) satisfies

$$\lambda_t \in \left[-\gamma \frac{T^{\max}(1 - \alpha)}{\min_{t'=1, \dots, t-1} p_{t'}^{\min}}, 1 + \gamma \frac{T^{\max} \alpha}{\min_{t'=1, \dots, t-1} p_{t'}^{\min}} \right], \quad (42)$$

as long as one selects $\lambda_1 \in [0, 1]$. Accordingly, we have

$$\frac{|\mathbb{E}[\lambda_{T+d_T+1}] - \lambda_1|}{\gamma} \leq \frac{1}{\gamma} + \frac{T^{\max}}{\bar{p}_{T+T^{\max}}}, \quad (43)$$

where

$$\bar{p}_{T+T^{\max}} = \min_{t'=1, \dots, T+T^{\max}} p_{t'}^{\min}. \quad (44)$$

This quantity does not depend on T if there exists $\bar{p} > 0$ such that

$$\bar{p}_{T+T^{\max}} \geq \bar{p} \quad (45)$$

for all times $T + T^{\max}$.

Combining (41) and (43), we obtain

$$C = T^{\max} - 1 + \frac{1}{\gamma} + \frac{T^{\max}}{\bar{p}_{T+T^{\max}}} \leq T^{\max} - 1 + \frac{1}{\gamma} + \frac{T^{\max}}{\bar{p}}, \quad (46)$$

which concludes the proof. \square

Acknowledgements

The work of M. Zecchin and O. Simeone is supported by the European Union's Horizon Europe project CENTRIC (101096379). The work of O. Simeone is also supported by an Open Fellowship of the EPSRC (EP/W024101/1), and by the EPSRC project (EP/X011852/1).

References

A. N. Angelopoulos, R. F. Barber, and S. Bates. Online conformal prediction with decaying step sizes. *arXiv preprint arXiv:2402.01139*, 2024.

- S. Bartels, J. Cockayne, I. C. Ipsen, and P. Hennig. Probabilistic linear solvers: A unifying view. *Statistics and Computing*, 29:1249–1263, 2019.
- S. P. Boyd and L. Vandenberghe. *Convex Optimization*. Cambridge University Press, 2004.
- J. Cockayne, C. J. Oates, I. C. Ipsen, and M. Girolami. A bayesian conjugate gradient method (with discussion). *Bayesian Analysis*, 14(3), 2019a.
- J. Cockayne, C. J. Oates, T. J. Sullivan, and M. Girolami. Bayesian probabilistic numerical methods. *SIAM review*, 61(4):756–789, 2019b.
- J. Cockayne, I. C. Ipsen, C. J. Oates, and T. W. Reid. Probabilistic iterative methods for linear systems. *Journal of machine learning research*, 22(232): 1–34, 2021.
- J. Cockayne, M. M. Graham, C. J. Oates, T. J. Sullivan, and O. Teymur. Testing whether a learning procedure is calibrated. *Journal of Machine Learning Research*, 23(203):1–36, 2022.
- S. Feldman, L. Ringel, S. Bates, and Y. Romano. Achieving risk control in online learning settings. *arXiv preprint arXiv:2205.09095*, 2022.
- G. J. Gassner and A. R. Winters. A novel robust strategy for discontinuous Galerkin methods in computational fluid mechanics: Why? When? What? Where? *Frontiers in Physics*, 8:500690, 2021.
- I. Gibbs and E. Candes. Adaptive conformal inference under distribution shift. *Advances in Neural Information Processing Systems*, 34:1660–1672, 2021.
- G. H. Golub and C. F. Van Loan. *Matrix Computations*. JHU press, 2013.
- D. Hegde, M. Adil, and J. Cockayne. Calibrated computation-aware Gaussian processes. In *The 28th International Conference on Artificial Intelligence and Statistics*, volume 258, 2025.
- P. Hennig, M. A. Osborne, and M. Girolami. Probabilistic numerics and uncertainty in computations. *Proceedings of the Royal Society A: Mathematical, Physical and Engineering Sciences*, 471(2179):20150142, 2015.
- Z. Hong, W. Chen, H. Huang, S. Guo, and Z. Zheng. Multi-hop cooperative computation offloading for industrial IoT–edge–cloud computing environments. *IEEE Transactions on Parallel and Distributed Systems*, 30(12): 2759–2774, 2019.
- G. W. Imbens and D. B. Rubin. *Causal Inference for Statistics, Social, and Biomedical Sciences*. Cambridge University Press, 2015.

- F. Larkin. Gaussian measure in Hilbert space and applications in numerical analysis. *Journal of Mathematics*, 2(3), 1972.
- M. Pförtner, I. Steinwart, P. Hennig, and J. Wenger. Physics-informed Gaussian process regression generalizes linear PDE solvers. *arXiv preprint arXiv:2212.12474*, 2022.
- M. Pförtner, J. Wenger, J. Cockayne, and P. Hennig. Computation-aware Kalman filtering and smoothing. *arXiv preprint arXiv:2405.08971*, 2024.
- T. W. Reid, I. C. F. Ipsen, J. Cockayne, and C. J. Oates. Statistical properties of BayesCG under the Krylov prior. *Numer. Math.*, 155(3-4):239–288, 2023.
- S. Thrun. Probabilistic robotics. *Communications of the ACM*, 45(3):52–57, 2002.
- J. Wenger and P. Hennig. Probabilistic linear solvers for machine learning. *Advances in Neural Information Processing Systems*, 33:6731–6742, 2020.
- J. Wenger, G. Pleiss, M. Pförtner, P. Hennig, and J. P. Cunningham. Posterior and computational uncertainty in Gaussian processes. *Advances in Neural Information Processing Systems*, 35:10876–10890, 2022.
- M. Zhao, R. Simmons, H. Admoni, A. Ramdas, and A. Bajcsy. Conformalized interactive imitation learning: Handling expert shift and intermittent feedback. *arXiv preprint arXiv:2410.08852*, 2024.